https://dx.doi.org/10.1016/j.epsr.2020.106704

Spurious Power and Its Elimination in Modular Multilevel Converter Models

Anton Stepanov[a]*, Hani Saad[b], Ulas Karaagac[c], Jean Mahseredjian[a]

[a] Polytechnique Montreal, Montréal, Canada.
[b] Réseau de Transport d'Electricité, Lyon, France.
[c] Hong Kong Polytechnic University, Hung Hom, Kowloon, Hong Kong.
*Corresponding author. Email address: anton.stepanov@polymtl.ca

ABSTRACT

This paper demonstrates the presence of spurious power generation or losses in two commonly used Modular Multilevel Converter (MMC) models: the Arm Equivalent Model (AEM) and the Average Value Model (AVM). Such power does not represent any physical phenomenon and appears due to numerical effects. It is demonstrated that spurious power is present when the model equations are not solved simultaneously with the surrounding electrical circuit equations, which is the case when the AEM and AVM are implemented using control system blocks. Depending on operating conditions and simulation parameters, such power can represent a significant part of the total converter station losses or even surpass them, thus making simulation results inaccurate. Several solutions to eliminate the spurious power are proposed for the AEM and AVM. Their effects are demonstrated in steady-state conditions on a point-to-point MMC-HVDC simulation test case.

Keywords: arm equivalent model, average value model, HVDC, modular multilevel converter, simulation.

1. Introduction

Modular Multilevel Converter (MMC) shown in Fig. 1 is a Voltage Source Converter (VSC) topology that has several advantages in comparison with conventional two- and three-level power electronic converters. Increasing the number of sub-modules (SMs) per arm helps reduce or eliminate filters, improve reliability, and easily achieve scalability to higher voltages. In addition, MMCs have lower losses, lower switching frequency, lower transient peak voltages on IGBTs, and lower switching voltages. During normal operation, the desired AC voltage waveform is constructed by inserting or bypassing the appropriate number of SMs [1].

Due to the increased structural complexity of this type of converter compared to the conventional VSCs, a larger set of models is applicable in electromagnetic transient (EMT) simulations, including the detailed model (DM), the detailed equivalent model (DEM), the arm equivalent model (AEM), and the average value model (AVM) [2]. The choice of the model depends on the given simulated phenomenon and is usually associated with a compromise between required accuracy and tolerable computational burden [3].

The DM representing nonlinear characteristics of IGBTs and diodes offers a very high accuracy. However, this model is the slowest due to the significant number of nodes and nonlinearities [3], [4]. The DEM simplifies the details of the nonlinear characteristics of power switches to only two states (ON and OFF) and uses Thevenin or Norton equivalent circuits to represent each converter arm, which considerably reduces computational burden [4].

The AEM hides individual SM details and deals with a single equivalent capacitor in each arm (see Fig. 2). This makes this model advantageous for a large set of grid studies where the converter behavior on SM level is disregarded [5]. The AVM combines all six arm capacitors into one, so only the external behavior of the converter is represented [4].

The MMC models can be implemented in different ways in an EMT-type software: the model equations can be incorporated into the main network equations (MNE) matrix, which eliminates the one-time-step delay between the model equations and the MNE. However, the main drawback is the inaccessibility of model equations to the user. Otherwise, the model equations can be implemented using control diagram blocks of the EMT software [6], [7]. In this case, the drawback is the one-time-step delay between the solution of control system equations and the MNE.

In this paper it will be analytically demonstrated that in the second approach (models in control blocks), additional spurious power can occur, that affects the overall behavior of the circuit and makes the simulation results less reliable. Such spurious power has been researched in [8] and [9] but only the AEM has been considered. This paper extends the spurious power analysis presented in [8] to the AVM, which is often used with large time-steps so considerable effects of the spurious power can be expected. Several solutions to remediate the problem are discussed. Proposed solutions are validated on a practical test case of a point-to-point MMC-based HVDC transmission system.

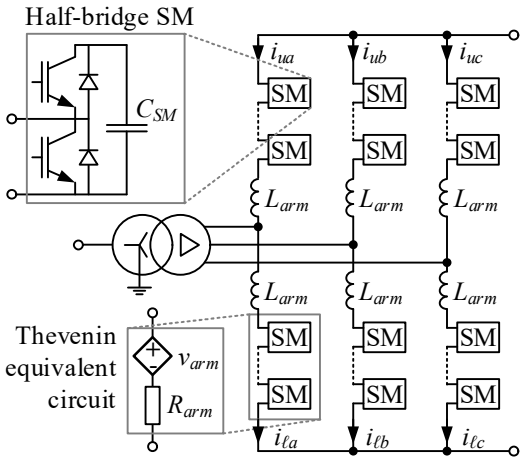

Fig. 1. Three-phase MMC topology with a coupling transformer

2. AEM Spurious Power in Steady-State

2.1. Normal Operation of Arm Equivalent Model

Two operation modes are usually discussed when dealing with MMCs: normal operation and blocked mode. In this paper, normal operation is of primary interest, because power losses are important in steady-state operation [10].

Considering an ideal AEM with lossless semiconductor devices, the basic equations of the model for a given arm during normal operation are as follows [2], [11] (hereafter, the time-varying signals are denoted with lowercase letters):

$$v_{arm} = s_{arm}\, v_{Ctot} \tag{1}$$

$$i_{Ctot} = s_{arm}\, i_{arm} \tag{2}$$

$$\frac{d}{dt} v_{Ctot} = \frac{i_{Ctot}}{C_{eq}} \tag{3}$$

$$C_{eq} = C_{SM} / N_{SM} \tag{4}$$

where s_{arm} is the arm switching function (i.e. proportion of inserted SMs to the total number of SMs in the arm), v_{arm} is the arm voltage, v_{Ctot} is the equivalent capacitor voltage, i_{arm} is the arm current, i_{Ctot} is the equivalent capacitor current, C_{eq} is the equivalent arm capacitor, C_{SM} is the SM capacitance, and N_{SM} is the number of SMs per arm.

If equations (1)–(3) are solved simultaneously at each time-point, the solution is perfectly accurate in terms of power

balance, as demonstrated below. Instantaneous arm power on the power circuit side is given by:

$$p_{arm} = i_{arm}\ v_{arm} \tag{5}$$

Instantaneous power on the equivalent capacitor side becomes:

$$p_{Ctot} = i_{Ctot}\ v_{Ctot} \tag{6}$$

The powers in (5) and (6) must be equal, because there is no other element that can consume, produce or store energy (as semiconductors losses are not considered in this equation). Considering (2), (6) can be rewritten as

$$p_{Ctot} = i_{arm}\ s_{arm}\ v_{Ctot} \tag{7}$$

When considering (1), (5), and (7) it is clear that $p_{arm} = p_{Ctot}$, so no spurious power is being generated or consumed irrespective of the waveforms of i_{arm} and v_{arm}.

Arm equations (1)–(3) can be implemented in an EMT-type simulation software in a form of a control circuit (Fig. 2). Semiconductor conduction losses can be modeled with a constant resistance [1], [2]:

$$R_{arm} = R_{ON}\ N_{SM} \tag{8}$$

where R_{ON} is the ON-state resistance of IGBT switches.

In this case, conduction losses can be expressed as

$$p_{cond} = R_{arm}\ i_{arm}^2 \tag{9}$$

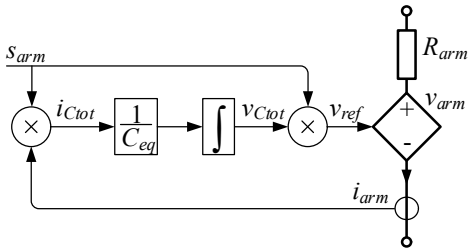

Fig. 2. Classical AEM schematic for normal operation mode.

2.2. Spurious Power Analysis in Arm Equivalent Model

In EMT-type software codes, it is usual to solve control system equations independently from the MNE, which results in a one-time-step delay between the two solutions.

2.2.1. AEM Spurious Power in Steady-State

The equivalent capacitor C_{eq} of the AEM can be implemented with control system blocks [6], [7] as shown in Fig. 2. In this case, there is a one-time-step (Δt) delay between v_{ref} (reference value from the control blocks) and v_{arm} (actual voltage):

$$v_{ref}(t) = v_{arm}(t + \Delta t) \tag{10}$$

Considering (10), (1) can be rewritten as

$$v_{arm}(t + \Delta t) = v_{ref}(t) = s_{arm}(t)\, v_{Ctot}(t) \tag{11}$$

Considering (11), (7) is rewritten as

$$p_{Ctot} = i_{arm}\ v_{ref} \tag{12}$$

The difference between p_{arm} and p_{Ctot} constitutes spurious power in one arm of the AEM Δp_{AEM}:

$$\Delta p_{AEM} = p_{arm} - p_{Ctot} \tag{13}$$

Introducing (5), (10), and (12) into (13):

$$\Delta p_{AEM}(t) = -i_{arm}(t)\left[v_{arm}(t + \Delta t) - v_{arm}(t)\right] \tag{14}$$

Clearly, as v_{arm} is not a constant value, the one-time-step delay between control blocks solution and MNE solution causes a difference between p_{arm} and p_{Ctot}, which results in overall spurious power losses or generation (if negative value).

2.2.2. Steady-State Behavior

Assuming that simulation time-step is small, the arm voltage derivative at a time-point t can be approximated by the finite difference:

$$\frac{d}{dt}v_{arm}(t) \approx \frac{v_{arm}(t+\Delta t)-v_{arm}(t)}{\Delta t} \tag{15}$$

With this, (14) can be rewritten to simplify steady-state analysis:

$$\Delta p_{AEM} \approx -\Delta t\, i_{arm}\frac{d}{dt}v_{arm} \tag{16}$$

For high-power MMCs used for HVDC transmissions, it is typical to have high number of levels and circulating current suppression control [12]. In this case, high-frequency components in arm voltages and currents can be neglected, and only DC and fundamental components will be considered in steady-state operation:

$$i_{arm}(t) = I_0 + I_1\cos(\omega t+\varphi_i) \tag{17}$$

$$v_{arm}(t) = V_0 + V_1\cos(\omega t+\varphi_v) \tag{18}$$

where I_0, I_1, V_0, and V_1 are the amplitudes of the DC and the fundamental components of current and voltage respectively, φ_i and φ_v are the corresponding phase angles, and ω is the grid frequency in rad/s.

Considering (18), the arm voltage derivative becomes

$$\frac{d}{dt}v_{arm} = \omega V_1\cos\left(\omega t+\varphi_v+\frac{\pi}{2}\right) \tag{19}$$

Combining (16), (17), and (19):

$$\Delta p_{AEM} \approx \Delta t\left[I_0 + I_1\cos(\omega t+\varphi_i)\right]\omega V_1\cos\left(\omega t+\varphi_v-\frac{\pi}{2}\right) \tag{20}$$

The above equation can be separated into three harmonic terms: DC component, fundamental component, and double-fundamental-frequency component:

$$\Delta p_{AEM} = \Delta t\,\omega\frac{V_1 I_1}{2}\cos\left(\varphi_v-\varphi_i-\frac{\pi}{2}\right)+2\,\Delta t\,\omega V_1 I_0\cos\left(\omega t+\varphi_v-\frac{\pi}{2}\right)+\Delta t\,\omega\frac{V_1 I_1}{2}\cos\left(2\omega t+\varphi_v+\varphi_i-\frac{\pi}{2}\right) \tag{21}$$

While undesirable, the presence of oscillating terms will not deteriorate steady-state power balance because all the extra-generated power during one half-cycle will be consumed during the other half-cycle. The constant term, however, is always present and affects the converter power balance.

2.2.3. Double-Fundamental-Frequency Spurious Power

The double-fundamental-frequency components in (21) for the lower arms of phases A, B, and C (denoted as Δp_2) are found as:

$$\Delta p_2^A = \Delta t\,\omega\frac{V_1 I_1}{2}\cos\left(2\omega t+\varphi_v+\varphi_i-\frac{\pi}{2}\right) \tag{22}$$

$$\Delta p_2^B = \Delta t\,\omega\frac{V_1 I_1}{2}\cos\left(2\omega t+\varphi_v-\frac{2\pi}{3}+\varphi_i-\frac{2\pi}{3}-\frac{\pi}{2}\right) \tag{23}$$

$$\Delta p_2^C = \Delta t\,\omega\frac{V_1 I_1}{2}\cos\left(2\omega t+\varphi_v+\frac{2\pi}{3}+\varphi_i+\frac{2\pi}{3}-\frac{\pi}{2}\right) \tag{24}$$

Under balanced conditions, the above three components sum up to zero due to the 120° phase shift in between them. The

same formulation applies to the upper arms, so Δp_2 has no effect outside of the MMC. However, depending on control strategies during grid unbalance [12], fundamentals of current and voltage can differ among phases, so it is possible that double-fundamental-frequency spurious power becomes visible outside the MMC.

2.2.4. Fundamental-Frequency Spurious Power

The DC components of current and voltage in upper and lower arms are identical in each phase, while the fundamental components have a 180° phase shift. Therefore, the fundamental components of spurious power in (21) in the lower and upper arm of one phase (denoted as Δp_1) are:

$$\Delta p_1^{low} = \Delta t\ \omega\ V_1\ I_0 \cos\left(\omega t + \varphi_v - \frac{\pi}{2}\right) \tag{25}$$

$$\Delta p_1^{up} = \Delta t\ \omega\ V_1\ I_0 \cos\left(\omega t + \varphi_v + \pi - \frac{\pi}{2}\right) \tag{26}$$

The powers in upper (25) and lower (26) arms cancel each other out since they are in phase opposition. The same formulation applies to other phases, so there is no effect on the external behavior of the converter even during grid unbalance, because unbalance between upper and lower arms in each phase is usually kept to a minimum.

2.2.5. Constant Spurious Power

The constant term of (21) is the source of power mismatch affecting the whole grid, which is an overall undesirable behavior. The average value of the spurious power (denoted as Δp_0) per arm is given by

$$\Delta p_0 = \Delta t\ \omega \frac{V_1\ I_1}{2} \cos\left(\varphi_v - \varphi_i - \frac{\pi}{2}\right) \tag{27}$$

Depending on the phases of the AC components of arm current and voltage, Δp_0 can be positive as well as negative, i.e. both power loss and generation can occur. In balanced conditions, Δp_0 is the same for all six arms, so its effects sum up and can be observed outside of the MMC. During unbalance, Δp_0 can differ among arms.

3. AVM Spurious Power in Steady-State

3.1. Normal Operation of Average Value Model

The AVM contains two electrical circuits, AC and DC, which are disconnected from each other [2]. The AC (29) and DC (30) side equations for the normal operation mode are:

$$C_{AVM} = 6C_{eq} \tag{28}$$

$$v_m = s_m\ v_{AVM} \tag{29}$$

$$i_{AVM} = \sum_m s_m\ i_m \tag{30}$$

where C_{AVM} is the DC side AVM capacitor; $m = A, B, C$ is the phase index; s_m are the modulation signals provided by the control system ($s_m \in [-0.5; 0.5]$).

When (29) and (30) are solved together simultaneously, which is the case when the AVM is implemented using three ideal transformers with variable ratios s_m, the power at the AC side of the AVM $p_{AVM\ AC}$ equals the power at the DC side of the AVM $p_{AVM\ DC}$:

$$p_{AVM\ AC} = \sum_m v_m\ i_m \tag{31}$$

$$p_{AVM\ DC} = i_{AVM}\ v_{AVM} \tag{32}$$

From (29) and (30) it can be deduced that

$$i_{AVM} = \left[v_A \, i_A + v_B \, i_B + v_C \, i_C \right] / v_{AVM} \tag{33}$$

and considering (31)–(33), it is clear that $p_{AVM\ AC} = p_{AVM\ DC}$.

However, the AVM implementation using ideal transformers with variable ratios is not a common choice in EMT simulations. More often, the AVM is implemented using controlled voltage sources at the AC side and a controlled current source at the DC side, as shown in Fig. 3 [2]:

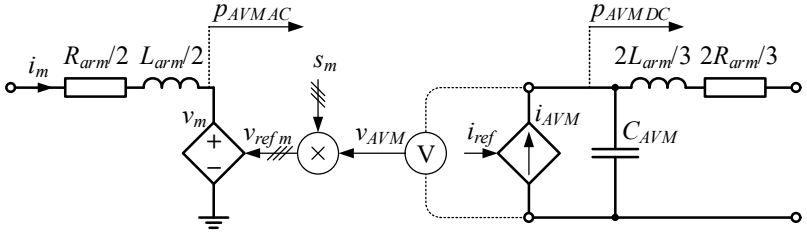

Fig. 3. AVM circuit for normal operation mode.

3.2. Spurious Power Analysis in Average Value Model

In the AVM implementation with controlled current and voltage sources, a difference between $p_{AVM\ AC}$ and $p_{AVM\ DC}$ can occur, indicating that some amount of active power is consumed or generated inside the converter. This is not realistic, and the difference constitutes the AVM spurious power:

$$\Delta p_{AVM} = p_{AVM\ AC} - p_{AVM\ DC} \tag{34}$$

With the Δt delay between solutions of the control system and the MNE, the AVM equations (29) and (30) become

$$v_m(t) = v_{ref\,m}(t - \Delta t) = s_m(t - \Delta t)\, v_{AVM}(t - \Delta t) \tag{35}$$

$$i_{AVM}(t) = i_{ref}(t - \Delta t) = \sum_m s_m(t - \Delta t)\, i_m(t - \Delta t) \tag{36}$$

In balanced steady-state conditions, the AVM voltage is considered constant:

$$v_{AVM}(t) = v_{AVM}(t - \Delta t) \tag{37}$$

so, considering (31), (32), and (35)–(37), the DC side power during normal operation can be rewritten as

$$p_{AVM\ DC}(t) = \sum_m v_m(t)\, i_m(t - \Delta t) \tag{38}$$

The phase currents in (38) are approximated with the first order derivative

$$i_m(t - \Delta t) \approx i_m(t) - \Delta t \frac{di_m(t)}{dt} \tag{39}$$

which results in the following equation for Δp_{AVM}:

$$\Delta p_{AVM} \approx \Delta t \sum_m v_m \frac{di_m}{dt} \tag{40}$$

Considering (17) and (18), the AC side voltages and currents can be written as (for phase A)

$$v_A(t) = V_1 \cos(\omega t + \varphi_v) \tag{41}$$

$$i_A(t) = 2I_1 \cos(\omega t + \varphi_i) \tag{42}$$

and additional $\mp 2\pi/3$ phase shifts are considered for the phases B and C, respectively.

Considering (40)–(42), Δp_{AVM} is rewritten as

$$\Delta p_{AVM} = 2\Delta t \, \omega \, V_1 \, I_1 \sum_m \cos(\Theta_{v\,m}) \cos(\Theta_{i\,m}) \tag{43}$$

where $\Theta_{v\,A} = \omega t + \varphi_v$ and $\Theta_{i\,A} = \omega t + \varphi_i + \pi/2$ are the angles for phase A voltage and current (and $\mp 2\pi/3$ phase shifts must be added for the phases B and C, respectively).

After applying trigonometric product formulas to (43), the steady-state equation of Δp_{AVM} in balanced AC grid conditions is obtained:

$$\Delta p_{AVM} = 3\Delta t\ \omega\ V_1\ I_1 \cos\left(\varphi_v - \varphi_i - \frac{\pi}{2}\right) \tag{44}$$

It can be seen that the instantaneous value of Δp_{AVM} in (44) is constant. Besides, the total spurious power in the converter is the same if it is modeled with AVM (44) or AEM (27) as long as the time-step, voltages and currents are the same:

$$\Delta p_{MMC} = 6\Delta p_0 = 3\Delta t\ \omega\ V_1\ I_1 \cos\left(\varphi_v - \varphi_i - \frac{\pi}{2}\right) = \Delta p_{AVM} \tag{45}$$

Considering (41) and (42), the reactive power consumed by the AC side controlled voltage sources can be expressed as $Q_{AVM\,AC} = 3\,I_1\,V_1 \sin\left(\varphi_v - \varphi_i\right)$. So, the AVM spurious power can also be expressed as

$$\Delta p_{AVM} = \Delta t\ \omega\ Q_{AVM\,AC} \tag{46}$$

During grid unbalance, negative sequence voltages and currents can appear, resulting in the double line frequency oscillations of the AVM spurious power (43). The active powers transmitted by phases can differ from each other in such conditions, so the double line frequency oscillations can appear at the DC side of the converter [12]. This would cause the AVM voltage v_{AVM} to oscillate and thus generate additional frequencies in Δp_{AVM} oscillations.

4. Elimination of Spurious Power

Four solutions to eliminate the spurious power are considered for the AEM: time-step reduction; extrapolating voltage references (extrapolation AEM); variable resistance AEM; equivalent voltage source AEM. Four solutions are proposed for the AVM: two extrapolation AVMs, power balance AVM and delayed AVM. Since the AVM is rarely used with small time-steps, the time-step reduction is not considered as a viable solution.

4.1. Time-Step Reduction

According to (20), spurious power in classical AEM depends on Δt, so reducing it will proportionally reduce Δp_{AEM}. Having maximal spurious power below or equal 10% of average conduction losses ($\overline{P}_{cond}$) can be considered as satisfactory reduction. In this case, the corresponding Δt can be found as:

$$\Delta p_{AEM} \le 10\%\ \overline{P}_{cond} \tag{47}$$

$$\Delta t\ \omega\ V_1\left[I_0 + I_1\right] \le 0.1\ R_{arm}\left[I_0^2 + I_1^2/2\right] \tag{48}$$

$$\Delta t \le 0.1\frac{R_{arm}\left[I_0^2 + I_1^2/2\right]}{\omega\ V_1\left[I_0 + I_1\right]} \tag{49}$$

With this criterion, for high-power HVDC transmissions where voltages are in the order of hundreds of kV and currents are in the order of kA, satisfactory reduction of spurious power can be achieved with time-steps not higher than 10 µs.

4.2. Extrapolation AEM

In steady-state and with relatively small simulation time-steps, arm voltage derivatives do not change significantly between adjacent time-points. This can justify a simple one-time-step extrapolation of the final voltage reference v_{ref}^{ext} supplied to the controlled voltage source:

$$v_{ref}^{ext} = v_{ref} + \Delta t \frac{d}{dt} v_{ref} \tag{50}$$

$$v_{arm}(t) = v_{ref}^{ext}(t - \Delta t) \tag{51}$$

The reference voltage derivative in (50) can be represented in the vicinity of time-point t using Taylor series (O represents higher-order terms):

$$v_{ref}(t) = v_{ref}(t - \Delta t) + \Delta t \frac{d}{dt} v_{ref}(t - \Delta t) + O(\Delta t^2) \tag{52}$$

Finally, (14) is rewritten as follows:

$$\Delta p_{AEM}(t) = i_{arm}(t)\left[v_{ref}^{ext}(t - \Delta t) - v^{ref}(t)\right] = i_{arm}(t)\, O(\Delta t^2) \tag{53}$$

In steady-state and with small time-steps, the second- and higher-order terms $O(\Delta t^2)$ are considerably smaller than the first-order derivative in (16), therefore Δp_{AEM} is significantly reduced. The derivative of the voltage reference in (50) can be approximated similarly to (15), so:

$$v_{ref}^{ext}(t) = 2 v_{ref}(t) - v_{ref}(t - \Delta t) \tag{54}$$

The corresponding implementation is shown in Fig. 4.

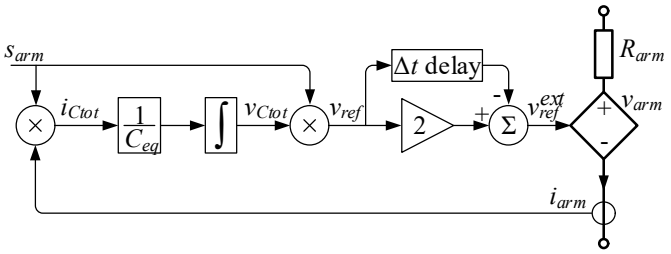

Fig. 4. Extrapolation AEM schematic.

4.3. Variable Resistance AEM

Another solution is to include a current-dependent summand in the calculation of arm voltage. Discretization of (3) using trapezoidal integration yields

$$v_{Ctot} = v_{hist\,Ctot} + R_C\, i_{arm}\, s_{arm} \tag{55}$$

with

$$v_{hist\,Ctot}(t + \Delta t) = v_{Ctot}(t) + R_C\, i_{arm}(t)\, s_{arm}(t) \tag{56}$$

$$R_C = 0.5\, \Delta t / C_{eq} \tag{57}$$

Multiplying both sides of (55) by s_{arm} and considering (1):

$$v_{arm} = R_C\, s_{arm}^2\, i_{arm} + s_{arm}\, V_{hist\,Ctot} \tag{58}$$

Since $v_{hist\,Ctot}$ and s_{arm} are known before the solution of MNE at the current time-point, implementation of (58) in the form of a Thevenin equivalent is straightforward:

$$v_{th} = v_{hist\,Ctot}\, s_{arm} \tag{59}$$

$$r_{th} = R_C\, s_{arm}^2 \tag{60}$$

In this case, (1)–(3) are solved simultaneously, so no spurious power occurs. Equations (55)–(60) can be implemented as shown in Fig. 5. This solution requires refactorization of MNE each time the value of r_{th} changes.

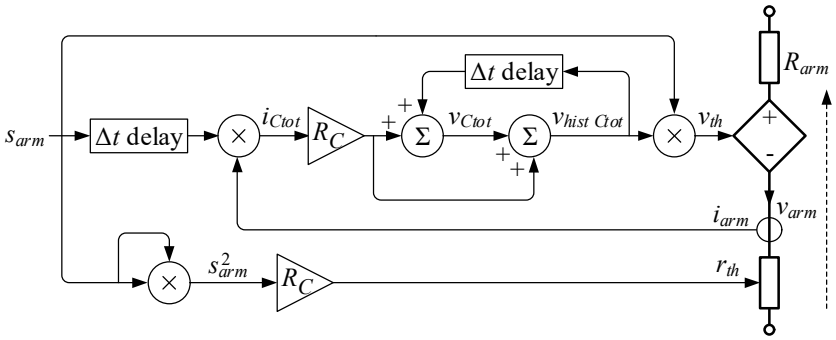

Fig. 5. Variable resistance AEM schematic.

The trapezoidal integration method is A-stable but prone to numerical oscillations if state variables experience discontinuities. Nevertheless, in this model such oscillations are avoided since the current i_{Ctot} does not depend on the state variable v_{Ctot} but is deduced from arm current i_{arm}.

4.4. Equivalent Voltage Source AEM

The main drawback of the variable resistance AEM presented in the section 4.3 is that it requires MNE refactorization every time the value of s_{arm} changes, which can happen at each time-point when Δt is relatively large. To overcome this inconvenience, the voltage drop on r_{th} can be emulated by an equivalent voltage source $v_{R\,eq}$ (61). In this case, the MNE matrix does not change so no refactorization is needed.

$$v_{R\,eq} = r_{th}\, i_{arm}^{ext} \tag{61}$$

where i_{arm}^{ext} is the extrapolated arm current.

Similarly to (54), extrapolated current can be obtained as:

$$i_{arm}^{ext}(t) = 2i_{arm}(t) - i_{arm}(t-\Delta t) \tag{62}$$

The corresponding implementation is shown in Fig. 6.

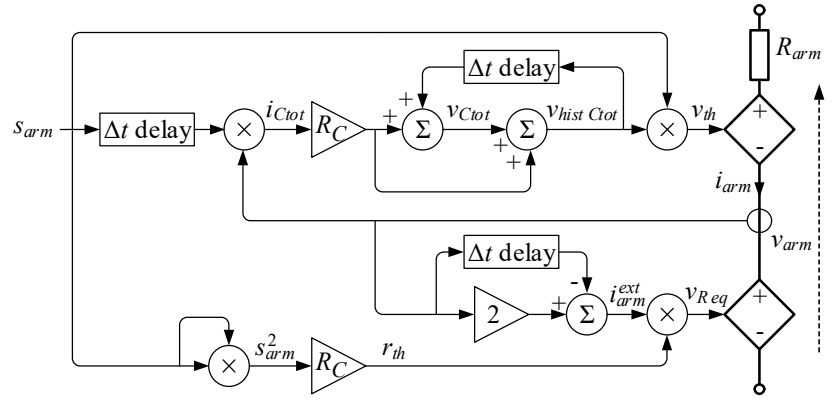

Fig. 6. Equivalent voltage source AEM schematic.

4.5. Extrapolation AVMs

Two possibilities for extrapolation are considered: the extrapolation can be applied either to the AC side voltage sources (only to the modulating signals s_m, since v_{AVM} is considered constant):

$$v_{ref\,m}(t) = v_{AVM}(t)\left[2s_m(t) - s_m(t-\Delta t)\right] \tag{63}$$

or to the phase currents for the DC side current source:

$$i_{ref}(t) = \sum_m s_m(t)\left[2i_m(t) - i_m(t-\Delta t)\right] \tag{64}$$

In both cases, the modulation signals taken to calculate the DC side current reference will correspond better to the values of AC side current than in the default implementation, which makes the DC current reference more accurate.

4.6. Power Balance AVM

Another solution to eliminate the spurious power in the AVM is to let the DC side current reference be explicitly defined by the power balance principle instead of using the modulating signals:

$$i_{ref} = \frac{p_{AVM\ AC}}{v_{AVM}} = \frac{1}{v_{AVM}} \sum_m v_m\ i_m \tag{65}$$

In this case, there is no spurious power as long as the AC side power and AVM capacitor voltage are constant, which is true for normal operation.

4.7. Delayed AVM

In this model, single time-step delays are added to the modulating signals in the equation for the DC current source reference (36) to make the modulating signals correspond to the AC side current instants, i.e. the modulating signals $s_m(t-\Delta t)$ that were used to obtain AC side voltages $v_m(t)$ and currents $i_m(t)$ at the instant t. In this case, the DC current reference becomes

$$i_{ref}(t) = \sum_m s_m(t-\Delta t)\, i_m(t) \tag{66}$$

Considering (35), the following can be written

$$i_{ref}(t) = \frac{1}{v_{AVM}(t-\Delta t)} \sum_m v_m(t)\, i_m(t) \tag{67}$$

It clear that this model is similar to the power balance AVM described in subsection 4.6 and will yield the same results as long as the AVM capacitor voltage is constant.

5. Test-Cases

A 401-level MMC-based HVDC link (Fig. 7) is used to validate the presented methods for eliminating spurious power. A standard cascade control system is used [3]. MMC1 controls active and reactive powers, MMC2 controls DC voltage and reactive power. System parameters are given in Table 1. DC cable model details can be found in [2]. All simulations are performed in EMTP [13].

Typically, station transformer losses represent 0.3% of the nominal power of the MMC P_{nom}. Converter losses are about 0.6% of the nominal power, they represent conduction and switching losses. Another 0.1% can be included for auxiliary and other high voltage equipment [10]. In this study, the total value for the losses represented by arm resistances is taken as 0.6%.

The ON-state resistance R_{ON} can be found from the equation of MMC losses (68) at nominal power transfer. The obtained value is 2.304 mΩ, which is realistic for high-power MMCs [14], [15].

$$P_{MMC} = 0.6\ P_{nom}\ /100 = 6\ N_{SM}\ R_{ON}\left[I_0^{\,2} + I_1^{\,2}/2\right] \tag{68}$$

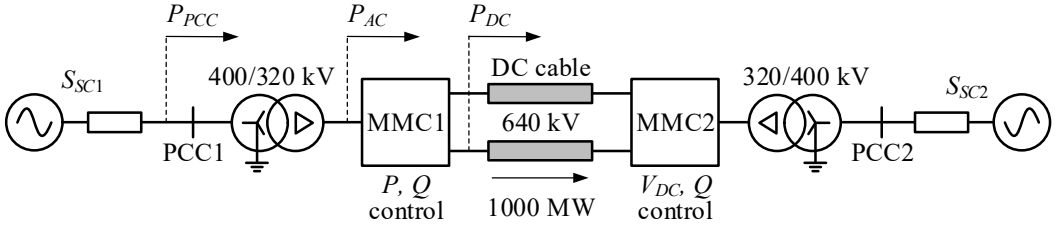

Fig. 7. Simulated point-to-point MMC-HVDC link.

Table 1. Simulation Parameters

Parameter	Nominal value	Symbol
Simulation time-step	50 µs	Δt
Grid frequency (both grids)	$2\pi \times 50$ rad/s	ω
Grid voltage (both grids)	400 kV	V_{AC}
Grid short-circuit level (both grids)	10 GVA	S_{SC}
DC voltage	640 kV	V_{DC}
Nominal MMC power (both stations)	1000 MW	P_{nom}
Number of SMs per arm (HB-SMs)	400	N_{SM}
DC voltage reference	1 pu	
Reactive power reference (both stations)	0 pu	
ON-state resistance of IGBTs & diodes	2.304 mΩ	R_{ON}
Arm inductance	0.15 pu	L_{arm}
Transformer resistance	0.004 pu	
Transformer inductance	0.18 pu	
Capacitor energy	40 kJ/MVA	

5.1. Demonstration of Spurious Power

To demonstrate the effects of spurious power, active powers at different points of the circuit are shown in Fig. 8 for the case of nominal power transfer using the classical AEM and AVM: at the point of coupling with the grid (P_{PCC}), at the AC terminals (P_{AC}), and at the DC terminals (P_{DC}) of the converter (see Fig. 7 for the location of these points). DEM is used as a reference model. In addition, adjusted power P_{adj} is shown in Fig. 8. This is the DC side power compensated for the spurious power:

$$P_{adj\ AEM} = P_{DC} + \sum_{m,n} \Delta p_{m,n} \tag{69}$$

$$P_{adj\ AVM} = P_{DC} + \Delta p_{AVM} \tag{70}$$

where $n = up, low$ denotes upper and lower arms.

With all models, the difference between P_{PCC} and P_{AC} is 3 MW, which corresponds to transformer losses (0.3% of the nominal power). However, visible difference exists between P_{DC} values. With the DEM, converter losses amount to approximately 6 MW (difference between P_{AC} and P_{DC}), which corresponds to 0.6% in (68). With the AEM and the AVM, the losses are considerably smaller. However, adjusted powers are at the same level as P_{DC} of the DEM, which confirms that spurious power is the source of the mismatch between P_{DC}.

It can also be observed that with the AVM all powers have smoother waveforms. This is because the AVM capacitor voltage is quasi-constant, contrary to more detailed models, where either arm capacitor voltages (AEM) or individual SM voltages (DEM) vary in time even in steady-state conditions.

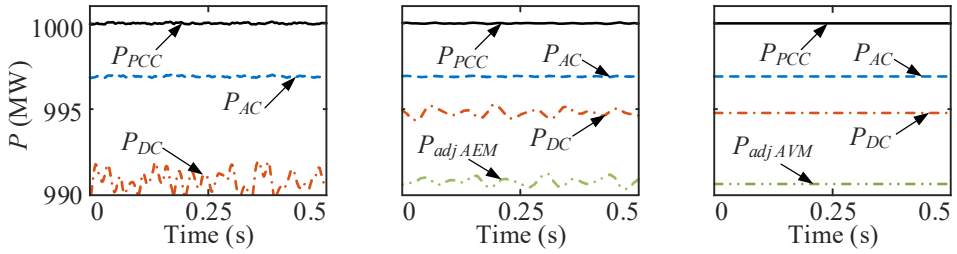

Fig. 8. Transmitted active powers at different points (see Fig. 7).

5.2. *Validation of Analytical Expression of Spurious Power*

To validate the analytical expression of spurious power, the HVDC link is subjected to nominal power transfer. The waveforms of Δp_{AEM} in the upper arm of phase A at MMC1 are shown in Fig. 9. Here Δp_{meas} is the measured value from the simulation and corresponds to (13), Δp_{calc} is the calculated value and corresponds to (21). Also, p_{cond} is shown in Fig. 9 to demonstrate how unwanted spurious power compares to the modeled losses. Measured and calculated waveforms of Δp_{AEM} match each other well and their values are considerably higher than conduction losses.

Table II shows the values of Δp_{AVM} and of Δp_{AEM} harmonics in phase A upper arm calculated using (22), (25), and (27) for different power angles φ_{ref} at PCC1 terminals (see Fig. 7). Analytical calculations match simulation results, which validates (21) and (44).

The same operating conditions are used to demonstrate linear dependency of the total spurious power in the converter Δp_{MMC} on Δt (see Fig. 10). Measured values (crosses for the AEM, circles for the AVM) match analytical predictions (lines). Depending on the operation mode, the spurious power can be positive or negative, indicating that power loss and generation can occur.

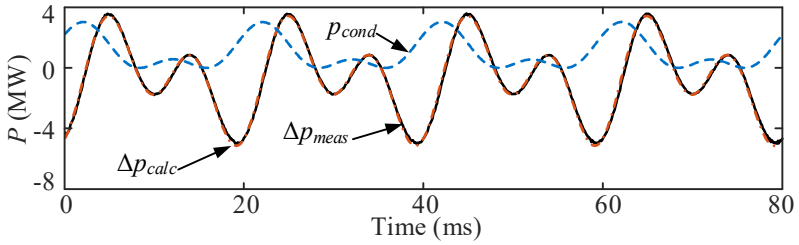

Fig. 9. AEM power in case of nominal power transfer.

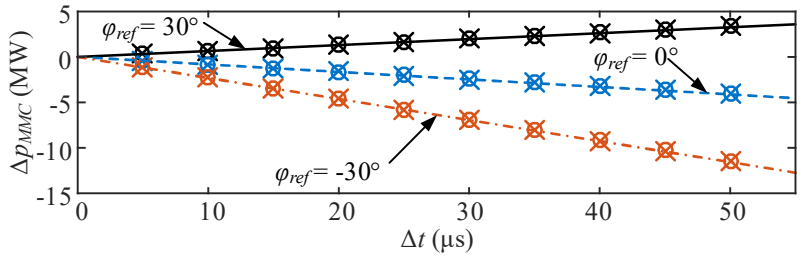

Fig. 10. Effect of Δt on total spurious power.

Table 2. Spurious Power in Different Operation Modes (MW)

Operation mode	Measures				Calculations			
	Δp_{AVM}	Δp_0	$\lvert\Delta p_1\rvert$	$\lvert\Delta p_2\rvert$	Δp_{AVM}	Δp_0	$\lvert\Delta p_1\rvert$	$\lvert\Delta p_2\rvert$
φ_{ref} = +30°	3.37	0.56	1.50	2.36	3.26	0.54	1.50	2.31
φ_{ref} = 0°	-4.01	-0.67	2.15	2.70	-4.13	-0.69	2.15	2.69
φ_{ref} = -30°	-11.5	-1.91	2.18	2.94	-11.6	-1.93	2.18	2.96

5.3. *Validation of Proposed Solutions*

Validation is performed using the HVDC link in Fig. 7 subjected to nominal power transfer. In the following subsections, Δp and p_{cond} in the upper arm of phase A at MMC1 are shown for the AEM validations to see how spurious power compares to the desired conduction losses with each solution. Since arm-level details are unavailable with AVMs, it is the total MMC converter losses p_{MMC} that are shown for the AVM validations.

5.3.1. Time-Step Reduction

The Δt calculated with (49) is approximately 1.5 µs. With this Δt, spurious power is smaller than conduction losses, but is still visible (see Fig. 11). The amplitude value is around 150 kW. Besides, the simulation is more than 30 times slower.

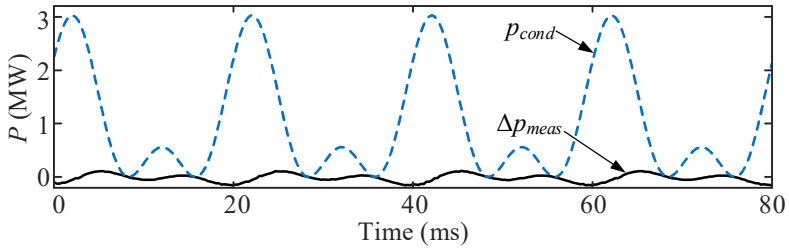

Fig. 11. AEM spurious power with Δt = 1.5 µs.

5.3.2. Extrapolation AEM

A one-time-step linear extrapolation is applied to the variable voltage source reference, as per subsection 4.2. Results are shown in Fig. 12. In this case, the spurious power is smaller than in the case of Fig. 11 but due to higher-order terms in (53) it is not exactly zero (around 100 kW). Simulations with Extrapolation AEM are about 2% longer than with the classical AEM.

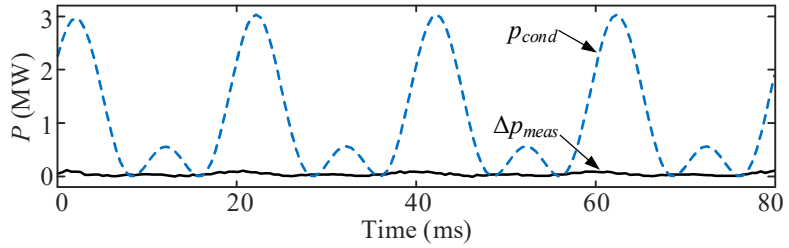

Fig. 12. Spurious power with extrapolation AEM.

5.3.3. Variable Resistance AEM

Variable resistance AEM is implemented as explained in subsection 4.3, results are shown in Fig. 13. With variable resistance, the spurious power is in the order of 10^{-7} W, which is negligible. Thus, this model achieves the highest possible accuracy. Due to MNE matrix refactoring, simulation time with this model is about 34% longer compared with the classical one.

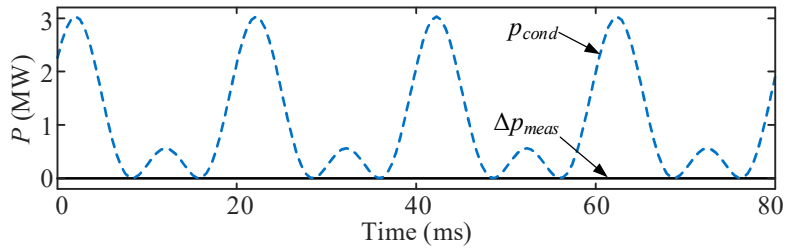

Fig. 13. Spurious power with variable resistance AEM.

5.3.4. Equivalent Voltage Source AEM

Equivalent Voltage Source AEM is implemented as explained in subsection 4.4, results are shown in Fig. 14. In this case, spurious power is below 1 kW, which is also negligible if compared to p_{cond}. Simulation time is about 10% larger than with the classical AEM implementation.

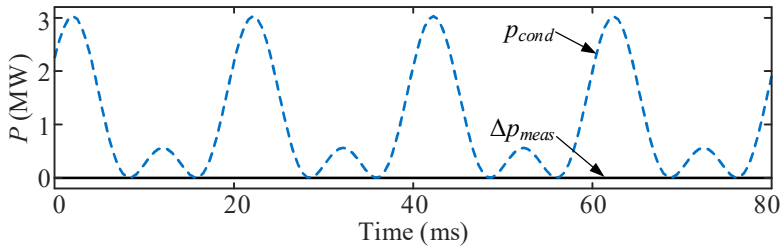

Fig. 14. Spurious power with equivalent voltage source AEM.

5.3.5. Extrapolation AVMs

Both extrapolation AVMs are implemented as explained in subsection 4.5, results are shown in Fig. 15. The spurious power with the voltage source extrapolation (63) $\Delta p_{v-extrap}$ and with the current source extrapolation (64) $\Delta p_{i-extrap}$ are both considerably lower than the total conduction losses in the converter but still perceivable (about 200 kW for the whole converter). Both extrapolation AVMs cause a slight increase in simulation time, about 2.5% from the default AVM.

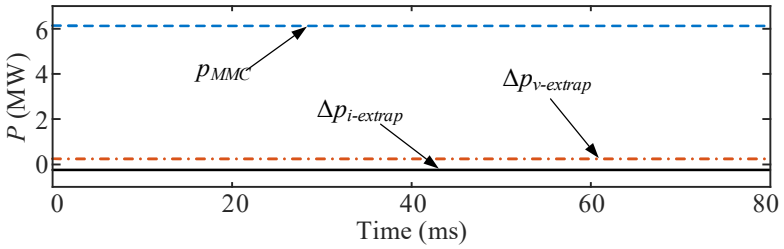

Fig. 15. Spurious power with extrapolation AVMs.

5.3.6. Power Balance AVM

The power balance AVM is implemented as explained in subsection 4.6, results are shown in Fig. 16. In this case, the spurious power is in the order of 1 W and can be neglected. With Power Balance AVM, simulation time increases by about 0.5% compared to the default AVM implementation.

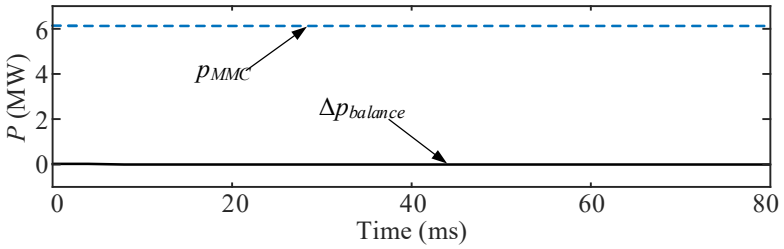

Fig. 16. Spurious power with power balance AVM.

5.3.7. Delayed AVM

The delayed AVM is implemented according to the subsection 4.7, results are shown in Fig. 17. In this case, the spurious power is also negligible, around 1 W. Simulation time is increased by about 2% with Delayed AVM when compared to the default implementation.

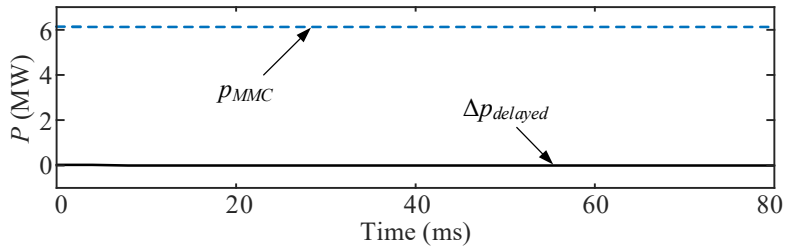

Fig. 17. Spurious power with delayed AVM.

5.4. Spurious Power During Transients

Spurious power with the proposed solutions during a 200 ms three-phase fault at PCC1 terminals is shown in Fig. 18 (AEMs) and Fig. 19 (AVMs). Since this paper only focuses on the normal operating mode of MMCs, DC fault behavior is excluded from the analysis because such faults promptly lead to the activation of the blocked mode.

In Fig. 18, Variable Resistance and Equivalent Voltage Source models keep the spurious power at very low levels whereas with Extrapolation AEM and Time-step Reduction AEM spurious power is in the order of tens of kilowatts during the transient.

In Fig. 19, the spurious power is practically identical with all proposed AVMs except the Current Extrapolation AVM and exhibits relatively large deviations from the steady-state value. This can be attributed to the fact that AVM capacitor voltage varies during the transient but is considered constant in all solutions except the Current Extrapolation AVM.

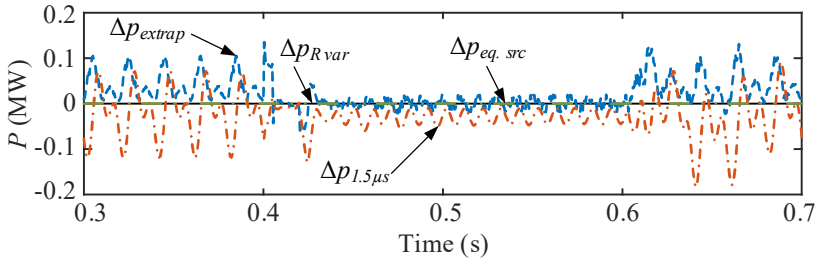

Fig. 18. Spurious power with proposed AEMs during a three-phase fault.

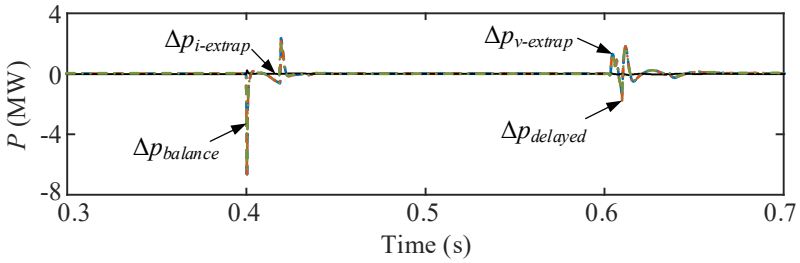

Fig. 19. Spurious power with proposed AVMs during a three-phase fault.

5.5. Solution Comparison

The advantages and disadvantages of all proposed solutions are summarized in the following table.

Table 3. Advantages and disadvantages of the proposed solutions

Model type	Name	Advantages	Disadvantages
AEM	Time-Step Reduction	No model modifications required	Slowest simulations and largest remaining spurious power
	Extrapolation	Minimal model modifications	Large remaining spurious power
	Variable Resistance	Zero remaining spurious power	MNE matrix refactorization
	Equivalent Voltage Source	Small remaining spurious power	Most complicated model
AVM	Current Extrapolation	Smallest spurious power during transient	Largest remaining spurious power
	Voltage Extrapolation		Largest remaining spurious power
	Power Balance	Smallest spurious power at steady-state	Large variations of spurious power during transient
	Delayed	Smallest spurious power at steady-state	Large variations of spurious power during transient

6. Acknowledgments

Anton Stepanov would like to acknowledge the support of Vanier Canada Graduate Scholarship in his research.

7. Conclusions

This paper demonstrates that spurious power loss or generation can occur when using the arm equivalent model or the average value model of MMC implemented in an EMT-type simulation software with control blocks. This is caused by the delay between solutions of electrical circuit and control system equations. Depending on the simulation conditions, such spurious power can represent a significant part of or even exceed total station losses, thus jeopardizing the accuracy of the simulations.

Analytical formulations of spurious power for both models are developed and validated in this paper. Several solutions to remove such power are proposed, and their effects are demonstrated on a point-to-point MMC-HVDC link. All solutions reduce spurious power to acceptable values. The presented solutions could also be applicable to other multilevel converters, such as cascaded multilevel converter.

8. References

[1] H. Saad, "Modélisation et simulation temps réel d'une liaison HVDC de type VSC-MMC," Ph.D. Thesis, Département de génie électrique, Polytechnique Montréal, Montreal, Canada, 2015.

[2] H. Saad, S. Dennetiere, J. Mahseredjian, P. Delarue, X. Guillaud, J. Peralta, and S. Nguefeu, "Modular Multilevel Converter Models for Electromagnetic Transients," *IEEE Trans. on Power Delivery,* vol. 29, pp. 1481-1489, June 2014.

[3] J. Peralta, H. Saad, S. Dennetiere, J. Mahseredjian, and S. Nguefeu, "Detailed and Averaged Models for a 401-Level MMC-HVDC System," *IEEE Trans. on Power Delivery,* vol. 27, pp. 1501-1508, July 2012.

[4] H. Saad, J. Peralta, S. Dennetiere, J. Mahseredjian, J. Jatskevich, J. A. Martinez, A. Davoudi, M. Saeedifard, V. Sood, X. Wang, J. Cano, and A. Mehrizi-Sani, "Dynamic Averaged and Simplified Models for MMC-Based HVDC Transmission Systems," *IEEE Trans. on Power Delivery,* vol. 28, pp. 1723-1730, July 2013.

[5] N. Ahmed, L. Angquist, S. Norrga, A. Antonopoulos, L. Harnefors, and H.-P. Nee, "A Computationally Efficient Continuous Model for the Modular Multilevel Converter," *IEEE Journal of Emerging and Selected Topics in Power Electronics,* vol. 2, pp. 1139-1148, Dec. 2014.

[6] H. Saad, K. Jacobs, W. Lin, and D. Jovcic, "Modelling of MMC including half-bridge and Full-bridge submodules for EMT study," *19th Power Systems Computation Conference, PSCC 2016*, Genova, Italy, June 2016, pp. 1-7.

[7] N. Ahmed, L. Ängquist, S. Norrga, H.-P. Nee, and 1, "Validation of the continuous model of the modular multilevel converter with blocking/deblocking capability," *10th IET International Conference on AC and DC Power Transmission (ACDC 2012)*, Birmingham, UK, Dec. 2012, pp. 1-6.

[8] A. Stepanov, H. Saad, U. Karaagac, and J. Mahserdjian, "Spurious Power Generation in Arm Equivalent Model Variants of Modular Multilevel Converter," *International Power Systems Transients Conference (IPST 2019)*, Perpignan, France, June 2019, pp. 1-6.

[9] A. Stepanov, H. Saad, U. Karaagac, and J. Mahseredjian, "Spurious Power Losses in Modular Multilevel Converter Arm Equivalent Model," *IEEE Transactions on Power Delivery,* vol. 35, pp. 205-213, 2020.

[10] IEC International Standard, "Power losses in voltage sourced converter (VSC) valves for high-voltage direct current (HVDC) systems – Part 2: Modular multilevel converters",115 p., 2014

[11] S. Norrga, L. Angquist, K. Ilves, L. Harnefors, and H. P. Nee, "Decoupled steady-state model of the modular multilevel converter with half-bridge cells," *6th IET International Conference on Power Electronics, Machines and Drives*, Stevenage, UK, Mar. 2012, pp. 1-6.

[12] A. Stepanov, H. Saad, J. Mahseredjian, and A. Wataré, "Overview of Generic HVDC-MMC Control under Unbalanced Grid Conditions," *International Power Systems Transients Conference (IPST 2017)*, Seoul, South Korea, June 2017, pp. 1-6.

[13] J. Mahseredjian, S. Dennetière, L. Dubé, B. Khodabakhchian, and L. Gérin-Lajoie, "On a new approach for the simulation of transients in power systems," *Electric Power Systems Research,* vol. 77, pp. 1514-1520, Sep. 2007.

[14] B4.57 CIGRE Working Group, "Guide for the Development of Models for HVDC Converters in a HVDC Grid",221 p., 2014

[15] S. Dennetière, "Contributions à la modélisation et à la validation des modèles de liaisons HVDC de type VSC-MMC dans les outils de simulation temps réel," Ph.D. Thesis, Département de génie électrique, Polytechnique Montréal, Montreal, Canada, 2017.